

Two-qubit silicon quantum processor with operation fidelity exceeding 99%

A. R. Mills,¹ C. R. Guinn,¹ M. J. Gullans,^{1,*} A. J. Sigillito,^{1,†} M. M. Feldman,¹ E. Nielsen,² and J. R. Petta¹

¹*Department of Physics, Princeton University, Princeton, New Jersey 08544, USA*

²*Sandia National Laboratories, Albuquerque, New Mexico 87185, USA*

Silicon spin qubits satisfy the necessary criteria for quantum information processing. However, a demonstration of high fidelity state preparation and readout combined with high fidelity single- and two-qubit gates, all of which must be present for quantum error correction, has been lacking. We use a two qubit Si/SiGe quantum processor to demonstrate state preparation and readout with fidelity over 97%, combined with both single- and two-qubit control fidelities exceeding 99%. The operation of the quantum processor is quantitatively characterized using gate set tomography and randomized benchmarking. Our results highlight the potential of silicon spin qubits to become a dominant technology in the development of intermediate-scale quantum processors.

Since the publication of the Loss-DiVincenzo proposal for spin-based quantum information processing in 1998 [1], the semiconductor quantum dot research community has worked to satisfy the DiVincenzo criteria for quantum information processing using spin qubits. Electron spins can be initialized and read out using spin-to-charge conversion [2, 3], single spin qubits can be coherently controlled using oscillating electromagnetic fields [4–6], and nearest neighbor spins can be coherently coupled via the exchange interaction [3].

Seminal results for spin qubits were obtained with GaAs quantum dots [2–4], however hyperfine coupling of the electron spin to lattice nuclei greatly limited quantum coherence [7]. A transition to silicon, which can be isotopically enriched, has led to a several order-of-magnitude increase in electron spin coherence times [8] as well as improved quantum control fidelities [9–11]. The small ~ 100 nm scale of quantum dot spin qubits and the significant capabilities of the silicon microelectronics industry could allow for scaling to system sizes that are capable of fault tolerant operation.

While high single- and two-qubit gate fidelities have been demonstrated in silicon [9, 11–13], state preparation and measurement (SPAM) errors have generally hovered around ~ 10 -20%. Here we demonstrate a spin-based two qubit quantum processor with all-around high performance fidelities (readout $F > 97\%$, simultaneous single qubit control $F > 99\%$, and a two-qubit controlled-phase (CPHASE) gate $F > 99.8\%$). Our two-qubit gate fidelity exceeds recent reports on spin qubits [12, 13] and is competitive with superconducting qubits [14, 15].

High-fidelity quantum control and readout are achieved in the first two qubits (Q1 and Q2) of a six qubit linear array [Fig. 1A]. Quantum dot electrons are vertically confined in an isotopically enriched (800 ppm) ²⁸Si quantum well and lateral confinement is achieved

using an overlapping aluminum gate stack [16]. Figure 1B depicts the double quantum dot formed under gates P1 and P2 with the exchange interaction controlled by gate B2 [3]. An external magnetic field $B_E = 365$ mT is applied in the plane of the quantum well to Zeeman split the spin-states. The external field adds to the magnetic field generated by a Co micromagnet resulting in electron spin resonance frequencies $f_1 = 18.247$ GHz and $f_2 = 17.851$ GHz.

We first demonstrate high visibility readout and single qubit control fidelities. Single qubit gates are achieved at the symmetric operating point in the (1,1) charge state using electric dipole spin resonance in the transverse field gradient created by the micromagnet [6, 17, 18]. Here (N_1, N_2) denotes the charge occupation of dots 1 and 2. Qubit state preparation and readout are achieved by spin dependent tunneling with the reservoir [2, 19, 20]. Figure 1C shows Rabi chevrons for each qubit, obtained by measuring the spin-up probability P_{\uparrow} as a function of drive frequency f and microwave burst length τ_R . Rabi oscillations approaching unit visibility are achieved when driving each qubit on resonance [Figure 1D].

We perform the quantum characterization, verification, and validation protocol of gate set tomography (GST) on the single qubit gates - identity (idle qubit i for $\pi/2$ gate time 70 ns) I_i , $\pi_X/2$ rotation X_i , and $\pi_Y/2$ rotation Y_i - and estimate single qubit control fidelities above 99.9% when driving and measuring one qubit at a time [Fig. 1C, inset] [21]. The fidelities are limited by decoherence [$T_2^*(T_2) = 1.7(23)$ μ s and $2.3(102)$ μ s for Q1 and Q2] and are comparable to the highest single spin qubit gate fidelities in the literature [9, 22]. SPAM errors extracted from GST are quantified by the initialization fidelities $\rho_{0,1} = 99.4\%$ and $\rho_{0,2} = 97.5\%$ and the measurement fidelities $M_1 = 98.1\%$ and $M_2 = 99.8\%$, making the overall operation fidelity high enough to support common error correction protocols.

Building to the two qubit space, we use GST to characterize the qubit control fidelities when both qubits are operated simultaneously ($X_1 \otimes X_2$, $Y_1 \otimes X_2$, etc.) by combining microwave control signals on the drive gate [MW gate in Fig. 1A]. GST estimates an average simultaneous single qubit control fidelity $F = 99.4 \pm 0.1\%$ when

* Present address: Joint Center for Quantum Information and Computer Science, NIST/University of Maryland, College Park, Maryland 20742, USA

† Present address: Department of Electrical and Systems Engineering, University of Pennsylvania, Philadelphia, Pennsylvania 19104, USA

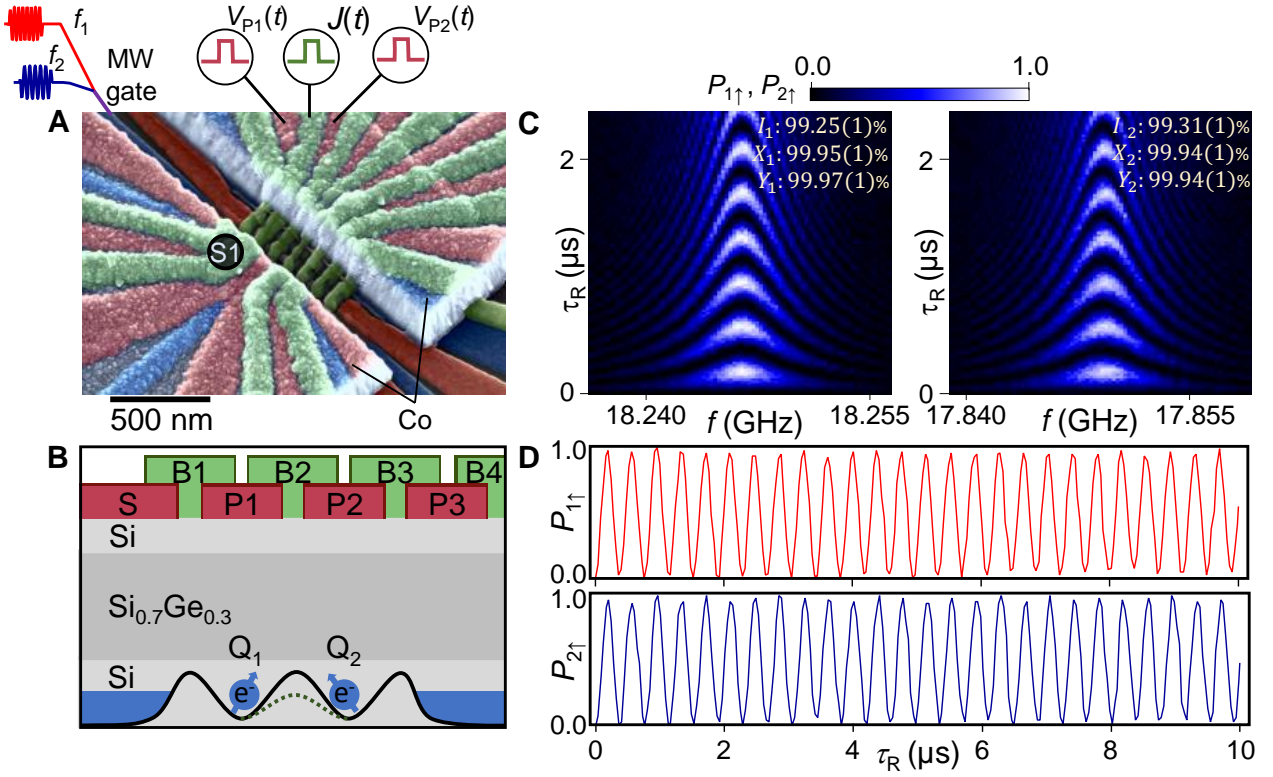


FIG. 1. **High-fidelity operation of a two-qubit quantum processor.** (A) False-color scanning electron microscope image of the device. Spins are selectively driven in a field gradient of a Co micromagnet using the microwave (MW) gate. (B) Two electron spins (Q_1 and Q_2) are trapped beneath gates P1 and P2, and the exchange coupling between the spins is set by the barrier gate B2. (C) Spin-up probabilities, $P_{1\uparrow}$ ($P_{2\uparrow}$), for Q_1 (Q_2) plotted as a function of drive frequency f and microwave burst length τ_R . Insets: Single qubit gate fidelities extracted from GST. (D) Spin-up probabilities for each qubit when driven on resonance.

operating in the two qubit space. Finally, we cross-check these GST results using the widely accepted protocol of randomized benchmarking (RB) and achieve $F_1 = 99.50 \pm 0.02\%$, $F_2 = 99.48 \pm 0.02\%$, and a joint fidelity of $99.13 \pm 0.03\%$. These results build significantly on past attempts to simultaneously drive spin qubits, where single qubit control fidelities were as low as 97% [10].

Two qubit control is achieved by pulsing on gate B2 to turn on the exchange interaction $J(V_{B_2})$ [3], which up to single qubit rotations yields a controlled-Z (CZ) gate $U_{CZ} = \text{diag}(1,1,1,-1)$ in the regime where the magnetic field gradient exceeds exchange $\Delta E_z \gg J$ [23, 24]. Figure 2A demonstrates a 3-decade variation of $J(V_{B_2})$. Exchange is extracted in the high- J regime ($J > 1/T_2^*$) by measuring time domain exchange oscillations [25], whereas a spin echo is utilized to measure residual exchange down to a T_2 limit of 10 kHz [blue in Fig. 2A]. In Fig. 2B we optimize the CZ gate by preparing the target qubit (Q_2 here) in a superposition state and the control qubit in either \uparrow or \downarrow . Exchange is then pulsed on for 40 ns using a smoothed square pulse [20] to execute a C-Phase gate. Afterwards, a software Z rotation Z_ϕ is applied to realize a CZ gate. As an initial demonstration of full two-qubit control with low SPAM errors, we perform Bell state tomography and use maximum likelihood estimation to

achieve the Bell state fidelities $|\Psi^+\rangle = 97.5\%(98.3\%)$, $|\Psi^-\rangle = 97.0\%(98.3\%)$, $|\Phi^+\rangle = 95.4\%(97.2\%)$, $|\Phi^-\rangle = 96.3\%(97.4\%)$, without (with) SPAM corrections included [Fig. 2C] [20]. These results significantly improve upon past measurements with SPAM corrected fidelities of 78-90% [11, 25–27] and are comparable to the *simulated* Bell state fidelities obtained by Xue *et al.* [12].

To demonstrate integrated control of the two qubit processor, we combine the CZ with other primitive qubit operations to create familiar two qubit gates (e.g. CNOT and SWAP). We first synthesize a CNOT gate using the Hadamard and CZ gates. Figure 3A shows the raw input-output measurement results of performing the synthesized CNOT gate on the four different input product states with Q_2 as the target. To show the target qubit will follow the control qubit state we prepare Q_1 in the \downarrow state and Q_2 in an arbitrary superposition state using a Rabi drive pulse for time τ_R . This state preparation routine is followed by the CNOT with Q_1 as the target qubit this time. The result is high visibility anti-correlated oscillations of the $\downarrow\downarrow$ and $\uparrow\uparrow$ joint state probabilities, Fig. 3B. Additionally, we generate synthesized SWAP gates with three alternating CNOT operations and measure the input-output SWAP table, Fig. 3C. To show a SWAP of an arbitrary superposition state $|\psi\rangle$ we perform a Rabi

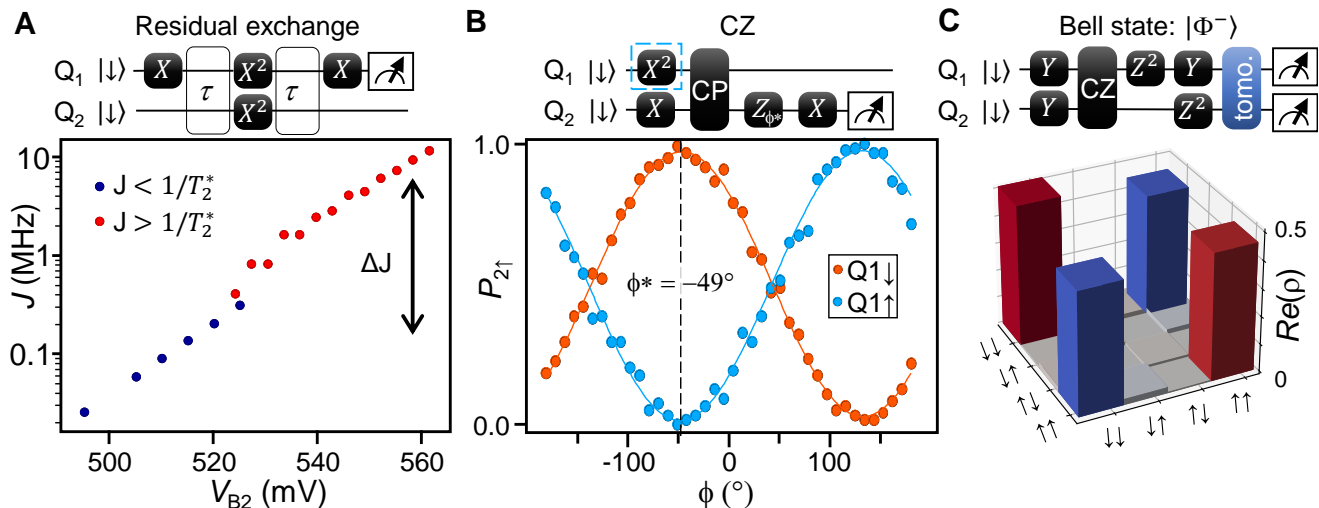


FIG. 2. **Optimization of the CZ gate.** (A) Exchange interaction measured as a function of V_{B2} using a combination of Ramsey and Hahn echo type sequences (see text). The quantity ΔJ indicates how far we can dynamically tune exchange. (B) The CZ is tuned by preparing the target spin in a superposition state, applying the C-Phase operation at $J \sim 5$ MHz for 40 ns, and then adjusting the phase Z_ϕ such that $P_{2\uparrow} = 1$ ($P_{2\uparrow} = 0$) when Q1 is prepared in the spin-down (spin-up) state using an optional π -pulse (blue dashed box). (C) Bell state tomography of the $|\Phi^-\rangle$ state yields the extracted density matrix (shown) with a raw state fidelity $F_u = 96.3\%$. Correcting for SPAM errors yields a fidelity $F_c = 97.4\%$.

drive pulse on Q2 and then SWAP the state onto Q1, resulting in Q2 being in the \downarrow state and Q1 in the $|\psi\rangle$ state [Fig. 3D].

We turn to two qubit interleaved RB to quantify the overall performance of our processor [28]. The two qubit Clifford group C_2 in this experiment has 576 single-qubit elements and integrates the CZ into 10944 two-qubit elements containing CNOT-, iSWAP-, and SWAP-like operations similar to those demonstrated in Fig. 3. With this technique, the CZ and synthesized CNOT fidelities can be determined by interleaving these operations in the benchmarking sequences and comparing to the reference curve. To thoroughly sample the Clifford group and obtain an accurate estimate of our CZ and CNOT fidelities we randomize 125 unique sequences for each reference and interleaved measurement going to sequence lengths as long as 65 total Clifford operations and average 160 times [Fig. 4]. The resulting two qubit RB fidelities for the CZ and CNOT are $F_{CZ} = 99.81 \pm 0.17\%$ and $F_{CNOT} = 98.62 \pm 0.16\%$ with error bars determined by bootstrapping [29].

We have demonstrated full two qubit control in a silicon quantum device with simultaneous single qubit control fidelities exceeding 99% and a primitive two-qubit CZ-gate fidelity exceeding 99.8%. In contrast to previous implementations [12, 13, 25, 26], SPAM errors are very low $< 3\%$. Our demonstration represents the highest total operation fidelity in a two qubit processor realized in silicon quantum dots with performance capable of fault tolerant operation [30]. These experiments demonstrate two qubit gates with silicon spin qubits at speeds exceeding trapped ions [31] and fidelities comparable with superconducting qubits [14, 15]. Given recent advances

in quantum dot fabrication [16, 32] spin qubits are poised to scale-up to larger multi-qubit quantum processors.

ACKNOWLEDGMENTS

We thank Remy Delva for computational support and David Zajac for assistance with sample fabrication. The Si/SiGe heterostructure used in these experiments was provided by HRL Laboratories, LLC. Supported by Army Research Office grant W911NF-15-1-0149 and DARPA grant D18AC0025. Devices were fabricated in the Princeton University Quantum Device Nanofabrication Laboratory, which is managed by the department of physics. The authors acknowledge the use of Princeton's Imaging and Analysis Center, which is partially supported by the Princeton Center for Complex Materials, a National Science Foundation MRSEC program (DMR-2011750). The Sandia National Laboratories part of this work was funded in part the by the U.S. Department of Energy, Office of Science, Office of Advanced Scientific Computing Research's Quantum Testbed Pathfinder. Sandia National Laboratories is a multimission laboratory managed and operated by National Technology and Engineering Solutions of Sandia, LLC, a wholly owned subsidiary of Honeywell International, Inc., for the U.S. Department of Energy's National Nuclear Security Administration under contract DE-NA0003525. All statements of fact, opinion or conclusions contained herein are those of the authors and should not be construed as representing the official views or policies of IARPA, the ODNI, the U.S. Department of

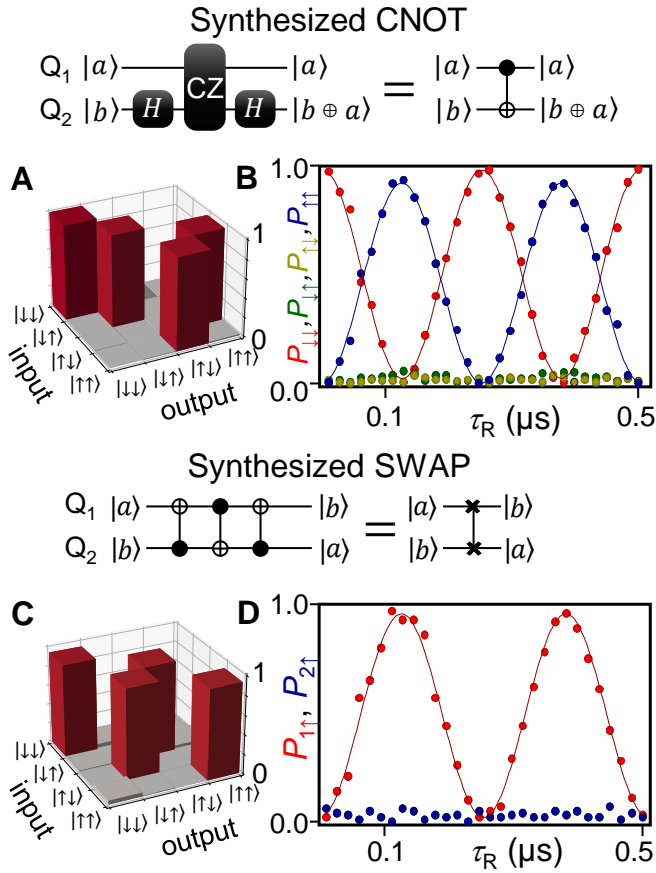


FIG. 3. **Synthesis of CNOT and SWAP gates using the primitive CZ gate.** (A) Input-output table illustrating the effect of the synthesized CNOT gate on the four different input product states ($|\uparrow\uparrow\rangle, |\uparrow\downarrow\rangle, |\downarrow\uparrow\rangle, |\downarrow\downarrow\rangle$). (B) Joint state probabilities $P_{\uparrow\uparrow}, P_{\uparrow\downarrow}, P_{\downarrow\uparrow},$ and $P_{\downarrow\downarrow}$ plotted as a function of microwave burst length τ_R at frequency f_2 showing that the joint state $|\downarrow\downarrow\rangle$ is anticorrelated with $|\uparrow\uparrow\rangle$. (C) Input-output table for the synthesized SWAP gate. (D) $P_{1\uparrow}$ and $P_{2\uparrow}$ measured as a function of Q2 drive time τ_R at frequency f_2 following a SWAP of the Q2 state onto Q1.

Energy, or the U.S. Government.

REFERENCES

[1] D. Loss and D. P. DiVincenzo, Quantum computation with quantum dots, *Phys. Rev. A* **57**, 120 (1998).
 [2] J. M. Elzerman, R. Hanson, L. H. W. Van Beveren, B. Witkamp, L. M. K. Vandersypen, and L. P. Kouwenhoven, Single-shot read-out of an individual electron spin in a quantum dot, *Nature* **430**, 431 (2004).
 [3] J. R. Petta, A. C. Johnson, J. M. Taylor, E. A. Laird, A. Yacoby, M. D. Lukin, C. M. Marcus, M. P. Hanson, and A. C. Gossard, Coherent manipulation of coupled electron spins in semiconductor quantum dots, *Science* **309**, 2180 (2005).
 [4] F. H. L. Koppens, C. Buizert, K.-J. Tielrooij, I. Vink, K. Nowack, T. Meunier, L. Kouwenhoven, and L. Van-

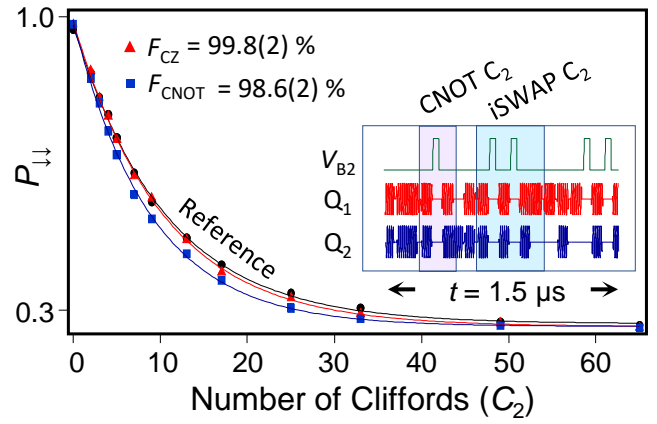


FIG. 4. **Two qubit interleaved RB.** Return probability $P_{\downarrow\downarrow}$ as a function of the number of two-qubit Clifford operations. Reference data are shown in black with error rate $r_{ref} = 0.0679$ [29]. Interleaved RB yields a two-qubit CZ fidelity $F_{CZ} = 99.8\%$ and synthesized CNOT fidelity $F_{CNOT} = 98.6\%$. Inset: Small portion of an RB sequence that includes a CNOT-like Clifford followed by an iSWAP-like Clifford.

dersypen, Driven coherent oscillations of a single electron spin in a quantum dot, *Nature* **442**, 766 (2006).

[5] K. C. Nowack, F. H. L. Koppens, Y. V. Nazarov, and L. M. K. Vandersypen, Coherent control of a single electron spin with electric fields, *Science* **318**, 1430 (2007).
 [6] M. Pioro-Ladriere, T. Obata, Y. Tokura, Y.-S. Shin, T. Kubo, K. Yoshida, T. Taniyama, and S. Tarucha, Electrically driven single-electron spin resonance in a slanting Zeeman field, *Nat. Phys.* **4**, 776 (2008).
 [7] R. Hanson, L. P. Kouwenhoven, J. R. Petta, S. Tarucha, and L. M. K. Vandersypen, Spins in few-electron quantum dots, *Rev. Mod. Phys.* **79**, 1217 (2007).
 [8] A. M. Tyryshkin, S. Tojo, J. J. L. Morton, H. Riemann, N. V. Abrosimov, P. Becker, H.-J. Pohl, T. Schenkel, M. L. W. Thewalt, K. M. Itoh, and S. A. Lyon, Electron spin coherence exceeding seconds in high-purity silicon, *Nat. Mater.* **11**, 143 (2012).
 [9] J. Yoneda, K. Takeda, T. Otsuka, T. Nakajima, M. R. Delbecq, G. Allison, T. Honda, T. Kodera, S. Oda, Y. Hoshi, N. Usami, K. M. Itoh, and S. Tarucha, A quantum-dot spin qubit with coherence limited by charge noise and fidelity higher than 99.9%, *Nat. Nanotechnol.* **13**, 102 (2018).
 [10] X. Xue, T. F. Watson, J. Helsen, D. R. Ward, D. E. Savage, M. G. Lagally, S. N. Coppersmith, M. A. Eriksson, S. Wehner, and L. M. K. Vandersypen, Benchmarking Gate Fidelities in a Si/SiGe Two-Qubit Device, *Phys. Rev. X* **9**, 021011 (2019).
 [11] W. Huang, C. H. Yang, K. W. Chan, T. Tanttu, B. Hensen, R. C. C. Leon, M. A. Fogarty, J. C. C. Hwang, F. E. Hudson, K. M. Itoh, A. Morello, A. Laucht, and A. S. Dzurak, Fidelity benchmarks for two-qubit gates in silicon, *Nature* **569**, 532 (2019).
 [12] X. Xue, M. Russ, N. Samkharadze, B. Undseth, A. Sammak, G. Scappucci, and L. M. K. Vandersypen, Computing with spin qubits at the surface code error threshold, *arXiv:2107.00628* (2021).
 [13] A. Noiri, K. Takeda, T. Nakajima, T. Kobayashi, A. Sam-

- mak, G. Scappucci, and S. Tarucha, Fast universal quantum control above the fault-tolerant threshold in silicon, [arXiv:2108.02626v2](https://arxiv.org/abs/2108.02626v2) (2021).
- [14] P. Mundada, G. Zhang, T. Hazard, and A. Houck, Suppression of qubit crosstalk in a tunable coupling superconducting circuit, *Phys. Rev. Applied* **12**, 054023 (2019).
- [15] Y. Sung, L. Ding, J. Braumüller, A. Vepsäläinen, B. Kannan, M. Kjaergaard, A. Greene, G. O. Samach, C. McNally, D. Kim, A. Melville, B. M. Niedzielski, M. E. Schwartz, J. L. Yoder, T. P. Orlando, S. Gustavsson, and W. D. Oliver, Realization of High-Fidelity CZ and ZZ-Free iSWAP Gates with a Tunable Coupler, *Phys. Rev. X* **11**, 021058 (2021).
- [16] D. M. Zajac, T. M. Hazard, X. Mi, E. Nielsen, and J. R. Petta, Scalable gate architecture for a one-dimensional array of semiconductor spin qubits, *Phys. Rev. Appl.* **6**, 054013 (2016).
- [17] M. D. Reed, B. M. Maune, R. W. Andrews, M. G. Borselli, K. Eng, M. P. Jura, A. A. Kiselev, T. D. Ladd, S. T. Merkel, I. Milosavljevic, E. J. Pritchett, M. T. Rakher, R. S. Ross, A. E. Schmitz, A. Smith, J. A. Wright, M. F. Gyure, and A. T. Hunter, Reduced sensitivity to charge noise in semiconductor spin qubits via symmetric operation, *Phys. Rev. Lett.* **116**, 110402 (2016).
- [18] F. Martins, F. K. Malinowski, P. D. Nissen, E. Barnes, S. Fallahi, G. C. Gardner, M. J. Manfra, C. M. Marcus, and F. Kuemmeth, Noise suppression using symmetric exchange gates in spin qubits, *Phys. Rev. Lett.* **116**, 116801 (2016).
- [19] M. Veldhorst, C. H. Yang, J. C. C. Hwang, W. Huang, J. P. Dehollain, J. T. Muhonen, S. Simmons, A. Laucht, F. E. Hudson, K. M. Itoh, A. Morello, and A. S. Dzurak, A two-qubit logic gate in silicon, *Nature (London)* **526**, 410 (2015).
- [20] Materials and methods are available as supplementary materials.
- [21] E. Nielsen, J. K. Gamble, K. Rudinger, T. Scholten, K. Young, and R. Blume-Kohout, Gate Set Tomography, *Quantum* **5**, 557 (2021).
- [22] C. H. Yang, K. W. Chan, R. Harper, W. Huang, T. Evans, J. C. C. Hwang, B. Hensen, A. Laucht, T. Tanttu, F. E. Hudson, S. T. Flammia, K. M. Itoh, A. Morello, S. D. Bartlett, and A. S. Dzurak, Silicon qubit fidelities approaching incoherent noise limits via pulse engineering, *Nat. Electron.* **2**, 151 (2019).
- [23] T. Meunier, V. E. Calado, and L. M. K. Vandersypen, Efficient controlled-phase gate for single-spin qubits in quantum dots, *Phys. Rev. B* **83**, 121403 (2011).
- [24] M. Russ, D. M. Zajac, A. J. Sigillito, F. Borjans, J. M. Taylor, J. R. Petta, and G. Burkard, High-fidelity quantum gates in Si/SiGe double quantum dots, *Phys. Rev. B* **97**, 085421 (2018).
- [25] T. F. Watson, S. G. J. Philips, E. Kawakami, D. R. Ward, P. Scarlino, M. Veldhorst, D. E. Savage, M. G. Lagally, M. Friesen, S. N. Coppersmith, M. A. Eriksson, and L. M. K. Vandersypen, A programmable two-qubit quantum processor in silicon, *Nature* **555**, 633 (2018).
- [26] D. M. Zajac, A. J. Sigillito, M. Russ, F. Borjans, J. M. Taylor, G. Burkard, and J. R. Petta, Resonantly driven CNOT gate for electron spins, *Science* **359**, 439 (2018).
- [27] R. C. C. Leon, C. H. Yang, J. C. C. Hwang, J. C. Lemyre, T. Tanttu, W. Huang, J. Y. Huang, F. E. Hudson, K. M. Itoh, A. Laucht, M. Pioro-Ladriere, A. Saraiva, and A. S. Dzurak, Bell-state tomography in a silicon many-electron artificial molecule, *Nat. Commun.* **12**, 3228 (2021).
- [28] E. Magesan, J. M. Gambetta, and J. Emerson, Scalable and robust randomized benchmarking of quantum processes, *Phys. Rev. Lett.* **106**, 180504 (2011).
- [29] R. Barends, J. Kelly, A. Megrant, A. Veitia, D. Sank, E. Jeffrey, T. C. White, J. Mutus, A. G. Fowler, B. Campbell, Y. Chen, Z. Chen, B. Chiaro, A. Dunsworth, C. Neill, P. O'Malley, P. Roushan, A. Vainsencher, J. Wenner, A. N. Korotkov, A. N. Cleland, and J. M. Martinis, Superconducting quantum circuits at the surface code threshold for fault tolerance, *Nature* **508**, 500 (2014).
- [30] A. G. Fowler, M. Mariantoni, J. M. Martinis, and A. N. Cleland, Surface codes: Towards practical large-scale quantum computation, *Phys. Rev. A* **86**, 032324 (2012).
- [31] C. D. Bruzewicz, J. Chiaverini, R. McConnell, and J. M. Sage, Trapped-ion quantum computing: Progress and challenges, *Appl. Phys. Rev.* **6**, 021314 (2019).
- [32] W. Ha, S. D. Ha, M. D. Choi, Y. Tang, A. E. Schmitz, M. P. Levendoff, K. Lee, J. M. Chappell, T. S. Adams, D. R. Hulbert, E. Acuna, R. S. Noah, J. W. Matten, M. P. Jura, J. A. Wright, M. T. Rakher, and M. G. Borselli, A flexible design platform for Si/SiGe exchange-only qubits with low disorder, [arXiv:2107.10916](https://arxiv.org/abs/2107.10916) (2021).